Bulletin of TICMI
Vol. 25, No. 01, 2021, 3–19

Turbulent Mixing Numerical Study in the Black Sea Basin Using Modified Version of the Pacanowski–Philander Formulation

Diana Kvaratskhelia[1,2*], Demuri Demetrashvili[1],
Khatuna Elbakidze[1,3,4,5], Luca SorrisoValvo[6,7]

[1] *M. Nodia Institute of Geophysics of I. Javakhishvili Tbilisi State University Tbilisi, Georgia*
[2] *Sokhumi State University, Tbilisi, Georgia*
[3] *I.Vekua Institute of Applied Mathematics of I. Javakhishvili Tbilisi State University Tbilisi, Georgia*
[4] *Black Sea International University, Tbilisi, Georgia*
[5] *Ilia State University, Tbilisi, Georgia*
[6] *Swedish Institute of Space Physics, Uppsala SE-751 05, Sweden*
[7] *CNR-Institute for the Science and Technology of Plasmas, via Amendola 124/D, 87036 Bari, Italy*

(*Received October 26, 2020; Revised December 28, 2020; Accepted January 28, 2021*)

In this paper, the Black Sea upper mixed layer (UML) structures in mid-February by using a 3-D numerical model of the Black Sea dynamics (BSM-IG, Tbilisi, Georgia) are investigated. In order to present the turbulent mixing peculiarities more clearly, a new version of the classical Pacanowski–Philander parameterization formulated by Bennis et al. (2010) for vertical turbulent viscosity and diffusion coefficients is integrated in the BSM-IG. The Black Sea UML homogeneity is estimated using criterion of temperature ($\triangle T = 0.2°C$) and salinity ($\triangle S = 0.15$ psu). Besides, mixed layer structures have been investigated according to both values of the Richardson number: Ri_T and Ri_S, respectively. As result analysis shows: in February UML structures in the temperature fields correspond to the Richardson number specificity, basically, but mixed layer homogeneity reduced in the salinity fields, when Richardson number changed in the following range $0.07 < Ri_S \leq 1$, especially, in deep waters of the sea basin.

Keywords: Black sea dynamics, Turbulent mixing, Homogeneous structures, Numerical integration, Numerical modeling.

AMS Subject Classification: 37N10, 35Q30, 76F25, 80M40, 80M20, 76F65, 37M05.

1. Introduction

It is well known, that the upper mixed layer (UML) in the sea and ocean plays a very important roles on the regional weather and climate change. This is mainly related to the turbulent sensible and latent heat fluxes, which are transferred from the marine UML into the atmosphere and make a significant contribution to the development of regional atmospheric processes. Besides, dynamical processes (circulation, wind-driven turbulence) in the upper layer play a significant role on the

*Corresponding author. Email: diana_kvaratskhelia@yahoo.com

ISSN: 1512-0082 print

nutrients spreading, which in turn is reflected on the living marine organisms. Except that, the light level for the tiny plants (e.g. phytoplankton's) metabolism is related on the mixed layer configuration (Oguz et al., 1999a, 2001a). Understanding of the nonlinear, non-stationary dynamical processes in the sea and ocean at the last decades has been progressed on the basis of the elaboration of several effective numerical models and rapid development of computer and observational technologies.

In this paper, our attention is focused on the upper layer of the Black Sea, many aspects of which in relation of dynamical processes (circulation, wind-driven turbulence, mixed layer forming, heat exchange, wave energy propagation) have been investigated by some authors on the basis of the various numerical models and by processing of measured data's (Friedrich and Stanev, 1988; Oguz et al., 1999a; Korotaev et al., 2003; Kara et al., 2005a, 2005c; Stanev, 2005; Kordzadze et al., 2008; Demetrashvili et al., 2008; Oguz, 2008; Helber et al., 2009; Korotaev et al., 2011; E. Rusu, 2011; Kubryakov et al., 2012; Capet et al., 2014; Pogrebnoi et al., 2014; Stanev et al., 2014; Mihailov et al., 2016; Ratner and Korotaev, 2017; Sukhik and Dorofeyev, 2018; Korotaev et al., 2018, Kvaratskelia et al., 2018; E. Rusu, 2018; Kubryakov et al., 2019, L. Rusu, 2019(1), 2019(2) and others).

The used physical models in context of the mixed layer study differ from each other by coordinate system, methods of solution, grid parameters, parametrization of turbulence and solar radiation penetration schemes (Friedrich and Stanev, 1988; Kara et al., 2005a, 2005c; Kordzadze et al., 2008; Korotaev et al., 2011, Stanev et al., 2014; Sukhik and Dorofeyev, 2018). Among them, here, we are concentrated on the 3-D basin-scale model of the Black Sea dynamics of M. Nodia Institute of Geophysics (BSM- IG, Tbilisi, Georgia), elaborated by Kordzadze et al. (2008). The use of this model, made it possible to study the non-stationary dynamical processes in the Black Sea basin (Kordzadze et al., 2008(1), 2008(2); Demetrashvili et al., 2008; Demetrashvili and Kvaratskhelia, 2012; Kvaratskhelia et al., 2018). Moreover, on the basis of BSM-IG at the Institute of Geophysics the high-resolution regional version (RM-IG) is successfully functioning in operational mode (Kordzadze and Demetrashvili, 2011; Demetrashvili et al., 2020), which was developed within the framework of international scientific projects ARENA and ECOOP (Korotaev et al., 2011; Kubryakov et al., 2012). The mentioned BSM-IG and RM-IG were operated in accordance to the constant values of vertical turbulent viscosity and diffusion coefficients and by modified Oboukhov formula (Marchuk et al., 1980), whose numerical values in the case of unstable stratication increasing 20 times, in the appropriate columns (Kordzadze et al., 2008; Kordzadze and Demetrashvili, 2011).

In order to present the properties of the turbulent mixed layer more clearly, the new version of classical Pacanowski and Philander (PP) Parameterization (1981), formulated by Bennis et al. (2010) for the vertical turbulent viscosity (VTV) and vertical turbulent diffusion (VTD) coefficients is integrated in the BSM-IG. This version excludes the numerical instability of the PP parametrization, which corresponds to physically unstable congurations (Bennis et al., 2008) taking place in the process of formation of the mixed layer.

The main object of this study is to numerically investigate the Black Sea UML physical structures homogeneity in the both temperature and salinity fields. In addition, the sensitivity of mixed-layer structures with regard to both values of the Richardson number: Ri_T and Ri_S, respectively, are main elements of our inves-

tigations. Here, the investigation of mixed layer features are presented for winter season, on an example of February, when above the Black Sea basin the relatively strong nonstationary atmospheric circulation and thermohaline actions are developed, basically.

Mixed layer depth (MLD) variability in the Black sea basin and its homogeneity in the simulated fields of temperature and salinity are determined using criterion of temperature ($\triangle T = 0.2°C$) and salinity ($\triangle S = 0.15\,\text{psu}$) (Thompson, 1976; Monterey and Levitus, 1997; Oguz et al., 2009). It should be noted that mixed layer using these criterion are defined as the depth, in which the variability of temperature and salinity from the sea surface till base of the upper mixed layer does not exceed 0.2°C and 0.15 psu respectively. In more detail, here in this paper, mixed layer homogeneity is defined by absolute values of the criterion of temperature and salinity.

2. Model description

The numerical experiment carried out using the 3-D, z-level numerical BSM-IG is based on a primitive system of ocean hydro and thermodynamics equations in the hydrostatic approximation (Kordzadze et. al., 2008).

The model equations system is represented as follows:

$$\frac{\partial u}{\partial t} + \operatorname{div}\vec{u}u - lv + \frac{1}{\rho_0}\frac{\partial p'}{\partial x} = \nabla\mu\nabla u + \frac{\partial}{\partial z}\nu\frac{\partial u}{\partial z} \tag{2.1}$$

$$\frac{\partial v}{\partial t} + \operatorname{div}\vec{u}v + lu + \frac{1}{\rho_0}\frac{\partial p'}{\partial y} = \nabla\mu\nabla v + \frac{\partial}{\partial z}\nu\frac{\partial v}{\partial z} \tag{2.2}$$

$$\frac{\partial p'}{\partial z} = g\rho' \tag{2.3}$$

$$\operatorname{div}\vec{u} = 0 \tag{2.4}$$

$$\frac{\partial T'}{\partial t} + \operatorname{div}\vec{u}T + \gamma_T w = \nabla\mu_T\nabla T' + \frac{\partial}{\partial z}\nu_T\frac{\partial T'}{\partial z} + \frac{\partial\nu_T\gamma_T}{\partial z} - \frac{1}{c\rho_0}\frac{\partial I}{\partial z} - \frac{\partial\overline{T}}{\partial t} \tag{2.5}$$

$$\frac{\partial S'}{\partial t} + \operatorname{div}\vec{u}S + \gamma_s w = \nabla\mu_S\nabla S' + \frac{\partial}{\partial z}\nu_S\frac{\partial S'}{\partial z} + \frac{\partial\nu_S\gamma_S}{\partial z} - \frac{\partial\overline{S}}{\partial t} \tag{2.6}$$

Here, $\rho' = \alpha_T T' + \alpha_S S'$, $\gamma_T = \frac{\partial\overline{T}}{\partial\overline{Z}}$, $\gamma_S = \frac{\partial\overline{S}}{\partial\overline{Z}}$,

$$T = \overline{T}(z,t) + T', \quad S = \overline{S}(z,t) + S', \quad \rho = \overline{\rho}(z,t) + \rho', \quad p = \overline{p}(z,t) + p',$$

$$\nabla\mu\nabla = \frac{\partial}{\partial x}\mu\frac{\partial}{\partial x} + \frac{\partial}{\partial y}\mu\frac{\partial}{\partial y},$$

$$\alpha_T = \partial f/\partial\overline{T} = -10^{-3}(0.0035 + 0.00938\overline{T} + 0.0025\overline{S}),$$

$$\alpha_S = \partial f/\partial\overline{S} = 10^{-3}(0.802 - 0.002\overline{T}),$$

$$I = \eta(1-A)I_0 e^{-\alpha Z}, \quad I_0 = a\sin h_0 - b\sqrt{\sin h_0},$$

$$\sin h_0 = \sin\varphi\sin\psi + \cos\varphi\cos\psi\cos\frac{\pi}{12}t,$$

$$\eta = 1 - (\widetilde{a} + \widetilde{b} \cdot \widetilde{n})\widetilde{n},$$

Here, u, v and w are the components of the current velocity vector $\vec{u}$ in the Cartesian coordinate system along axes x, y, z (the axis x is directed eastward, y northward, z from a sea surface vertically downwards), T', S', P', ρ' are deviations of temperature, salinity pressure and density from their standard vertical distributions . In this system the coefficients α_T and α_S are determined from the equation of state $\rho = f(T, S)$, specified by Mamaev formula (1964); I_0 is the total solar radiation flux at $z = 0$ determined by the Albrecht formula (Budyko, 1956). Values of other parameters and coefficients are described by Kordzadze et al. (2008), but the values of variable coefficients of VTV and VTD are given in the next subsection.

BSM-IG takes into account: quasi-realistic sea bottom relief, nonstationary atmospheric wind and thermohaline forcing, water exchange with the Mediterranean Sea and inflow of the Danube River, the absorption of solar radiation by the sea surface layer, space-temporal variability of horizontal and vertical turbulent viscosity and diffusion. Atmospheric forcing is taken as Neumann boundary conditions on the sea surface (considered as a rigid surface). On the sea bottom the velocity components, heat and salt fluxes are equal to zero. On the lateral surfaces, two kinds of boundary conditions are considered: a) on the rigid boundaries sharing sea from land, components of current velocity, gradients of temperature and salinity normal to the boundary surface are equal to zero; b) on the liquid boundaries connecting the sea with the Bosphorus Strait and the Danube River, values of velocity, temperature and salinity are given on the basis of experimental data. The annual mean climatic fields of current, temperature, and salinity obtained by the same BSM-IG are used as initial conditions. For this purpose, model equation system was integrated by zero initial conditions prior to reaching a quasi-stationary regime using mean annual climatic input data (Kordzadze et al., 2008).

3. Parameterization of the VTV and VTD processes

As mentioned, the variable coefficients of the VTV and VTD are included in the BSM-IG as a new version of classical PP parameterization, developed by Bennis et al. (2010). This version, in contrast to the original PP version and the later Ghent model (Bennis et al., 2008), in terms of the gradient Richardson number is stable in the computational process, when the ratio between stabilizing buoyancy forces and de-stabilizing shear forces is characterized by $R_i < 0$ (Bennis et al., 2010).

During the investigation, the total vertical eddy viscosity coefficient-ν is integrated in this model as function of the gradient Richardson number $\nu = f(Ri) = a_1 + \frac{b_1}{(1+\alpha Ri)^2}$ (Bennis et al., 2010). Richardson number Ri, defined as $Ri = \frac{g}{\rho_0} \frac{\partial_z \rho}{(\partial_z u)^2 + (\partial_z \nu)^2}$. The vertical turbulent diffusion coefficients for the temperature and salinity-ν_T and ν_S are calculated on the basis of the same formulas Bennis et al. (2010), which are presented as following: $\nu_T = a_2 + \frac{f(Ri_T)}{(1+\alpha Ri_T)^2}$ and $\nu_S = a_2 + \frac{f(Ri_S)}{(1+\alpha Ri_S)^2}$, respectively. Here, Richardson numbers Ri_T, Ri_S simulated through sea water temperature and salinity profiles: $Ri_T = \frac{g}{T} \frac{\partial_z T}{(\partial_z u)^2 + (\partial_z v)^2}$ and $Ri_S = \frac{g}{S} \frac{\partial_z S}{(\partial_z u)^2 + (\partial_z v)^2}$, respectively.

The mentioned model of Bennis et al.(2010) has been used successfully in the

algebraic oceanic turbulent mixing-layer model by Chacón–Rebollo et al. (2013, 2014). In our experiment, we used the same constants of PP parametrization: $a_1 = 1$, $a_2 = 0.1$, (units: $\mathrm{cm^2 s^{-1}}$), $b_1 = 50\,\mathrm{cm^2 s^{-1}}$. The α parameter is selected according to the Richardson number changes during model integration as following:

$$\alpha = \begin{cases} 0.001, & 100 \le R < 1000 \\ 0.01, & 10 \le R < 100 \\ 0.1, & 1 \le R < 10 \\ 1, & 0.1 \le R < 1 \\ 5, & 0.01 \le R < 0.1 \\ 10, & 0 < R < 0.01. \end{cases}$$

Such a selection of the values of the α adjustable parameter for various ranges of Richardson number, regulates the coefficients of viscosity and diffusion and ensures their values close to the experimental data in UML.

4. The solution method of the model equations system and integration of Bennis et al.(2010) formulation in BSM-IG

To solve the model equations system (2.1)–(2.6) a two-cycle method of splitting with respect to both physical processes and coordinate planes and lines is used (Marchuk, 1974). The main numerical techniques to solving the model equations system are basic methods of numerical analysis, such as: finite-difference approximation, absolutely stable scheme of Kranck-Nicholson, as well as factorization and upper relaxation methods (Marchuk, 1974, 1980). Here, three stages are presented after splitting of the model equations system on physical processes, which are solved on each double time step $t_{j-1} \le t \le t_{j+1}$.

1. In the first stage, on the time interval $t_{j-1} \le t \le t_j$ the transfer of physical fields is allocated taking into account eddy viscosity and diffusion:

$$\frac{\partial u_1}{\partial t} + \operatorname{div} \vec{w^j} u_1 = \frac{\partial}{\partial x}\mu\frac{\partial u_1}{\partial x} + \frac{\partial}{\partial y}\mu\frac{\partial u_1}{\partial y} + \frac{\partial}{\partial z}\nu\frac{\partial u_1}{\partial z} \tag{4.1}$$

$$\frac{\partial v_1}{\partial t} + \operatorname{div} \vec{w^j} v_1 = \frac{\partial}{\partial x}\mu\frac{\partial v_1}{\partial x} + \frac{\partial}{\partial y}\mu\frac{\partial v_1}{\partial y} + \frac{\partial}{\partial z}\nu\frac{\partial v_1}{\partial z} \tag{4.2}$$

$$\frac{\partial T_1}{\partial t} + \operatorname{div} \vec{w^j} T_1 = \frac{\partial}{\partial x}\mu_T\frac{\partial T_1}{\partial x} + \frac{\partial}{\partial y}\mu_T\frac{\partial T_1}{\partial y} + \frac{\partial}{\partial z}\nu_T\frac{\partial T_1}{\partial z} + \frac{\partial \nu_T \gamma_T}{\partial Z} \tag{4.3}$$

$$\frac{\partial S_1}{\partial t} + \operatorname{div} \vec{w^j} S_1 = \frac{\partial}{\partial x}\mu_S\frac{\partial S_1}{\partial x} + \frac{\partial}{\partial y}\mu_T\frac{\partial S_1}{\partial y} + \frac{\partial}{\partial z}\nu_S\frac{\partial S_1}{\partial z} + \frac{\partial \nu_S \gamma_S}{\partial Z}, \tag{4.4}$$

2. The second stage is the adaptation stage of the physical fields on the time interval $t_{j-1} \le t \le t_{j+1}$, where the following equations system is solved:

$$\frac{\partial u_2}{\partial t} - l v_2 + \frac{1}{\overline{\rho}}\frac{\partial p_2}{\partial x} = 0, \tag{4.5}$$

$$\frac{\partial v_2}{\partial t} + l u_2 + \frac{1}{\overline{\rho}}\frac{\partial p_2}{\partial y} = 0, \tag{4.6}$$

$$\frac{\partial p_2}{\partial t} = g(\alpha_T T_2 + \alpha_S S_2), \tag{4.7}$$

$$\frac{\partial u_2}{\partial x} + \frac{\partial v_2}{\partial y} + \frac{\partial w_2}{\partial z} = 0, \tag{4.8}$$

$$\frac{\partial T_2}{\partial t} + \gamma_T w_2 = 0, \tag{4.9}$$

$$\frac{\partial S_2}{\partial t} + \gamma_S w_2 = 0, \tag{4.10}$$

3. Finally, on the third stage within time interval $t_j \le t \le t_{j+1}$ the same transfer-diffusion equations are solved for functions u_3, v_3, w_3, p_3, T_3 and S_3.

On the basis of the numerical algorithm presented by Marchuk (1974), the equation systems in the first and third stages, in turn, are splitting with respect to spatial coordinates. The solution of nonstationary 3D problems are reduced to the solution of a set of simple second-order one-dimensional finite-difference equations. These equations, in finally are solved using the factorization method. In the second stage, adaptation phase of physical processes also uses splitting of equations with respect to spatial coordinates according which barotropic and baroclinic components of the adaptation are allocated. After using finite-difference approximation, the same Baroclinic problem splits on the zx and zy planes and set of 2-D problems for Baroclinic components, as in the Barothropic part, are reduced to the equations for analogs of the stream functions. The one-dimensional tasks obtained at the adaptation stage are solved using the upper relaxation method. As mentioned, for approximation on time of all split problems the Krank-Nickolson scheme is used (Marchuk, 1974, 1980).

It should be noted that the initial values of both VTV and VTD coefficients are constant: the VTV coefficient equal to $50\,\mathrm{cm^2 s^{-1}}$ in the upper layer of the Black Sea ($z \le 56\,\mathrm{m}$), but in the lower layer ($z > 56\,\mathrm{m}$) it is equal to $10\,\mathrm{cm^2 s^{-1}}$. In same times, VTD coefficient equal to $10\,\mathrm{cm^2 s^{-1}}$ from sea surface to a bottom. The model Bennis et al., (2010) is integrated 2 hours late, in the first and third stages of the model equations system and the values of the VTV and VTD coefficients are changed on each double time step ($t_{j-1} \le t \le t_{j+1}$) during integration. The software of the problem is developed on the basis of the algorithmic language Compaq Visual Fortran 6.1. It should be noted, that the formulation developed by Bennis group is successfully integrated in the BSM-IG.

5. Key model parameters

BSM-IG is operated with 5 km spacing on horizons having 225×111 points along axes x and y respectively. On a vertical the non-uniform grid with 34 calculated levels on different depths: 0, 2, 4, 6, 8, 12, 16, 26, 36, 56, 86, 136, 206, 306, . . . , 2306m were considered. The time step is equal to 1h. This numerical investigation carried out on the basis of several climatic data. The types of non-stationary atmospheric circulation is taken from (Atlas of excitement and wind of the Black Sea, 1969; Kordzadze et al., 2000). The multiyear monthly means profiles of the temperature and salinity (correspond to the period 1955-1994) were obtained from Department of Oceanology of M. Lomonosov Moscow State University. The climatic data of the heat fluxes, evaporation and atmospheric precipitation (Staneva et al., 1998), were

conveyed from the Marine Hydrophysical Institute (MHI, Sevastopol).

6. Results and discussion

The model integration started on the 1^{st} of January at 12:00h and proceeded for one modelling year. Here, mixed layer main element for winter season is presented in mid-February, corresponding to the time interval: 14^{st} of February, 24:00 h–17^{st} of February, 10:00h. This time period in the model is characterized by action of the relatively strong south-east (10–15 m/s) and south-west (10–15 m/s) winds corresponding to the following time intervals: 14^{st} of February, 24:00 h–15^{st} of February, 22:00h and 16^{st} of February, 6:00 h–17^{st} of February, 10:00h. Unlike they within the time period: 15^{st} of February, 22:00 h–16^{st} of February, 6:00h the calm-south wind (0–1 m/s) is functioned in the model. Besides, in February, according to base of climatic data, the heat flux is directed from the sea to the atmosphere, especially in the open part of the sea, above of 43°N more intensity, than in the other areas of sea basin. In the same active areas, evaporation is more than precipitation also. Before considering the results of numerical experiment, it should be noted, that in February, mixed layer in the Black sea basin is characterized by maximal depth using the sigma-t(density) criterion, 0.07 kg/m^3 (Kubryakov et al., 2019). Here in this study, same tendency, MLD increases especially in the temperature fields compared to January, is observed (Kvaratskhelia et.al., 2018).

The simulated fields of the sea current, temperature and salinity, in the different horizons within the depth of 0–60m, are presented on Figures 1, 2, at the time interval: 14^{st} of February, 24:00 h–17^{st} of February, 10:00h, characterize main hydrological peculiarities, which are developed in the upper layer of the sea basin in mid-February. As numerical experiment show, at the time moment: 22:00h, 15 February and 10:00h, 17 February, when above the Black Sea the strong south east and south-west winds are operated, sea circulation in the upper layer 0–8 meter significantly differ from each other (see Fig. 1). They in both cases are in the process to forming as the cyclonic current system. Below 16 meter, the Rim current with the internal cyclonic vortices are observed mainly. It should be noted that sea current has almost same structure within the depth 2–56m on 6:00h, 16 February, when calm south wind (0–1 m/s) operated in the model (Fig. 1). The transformation of sea circulation connected with the nonstationary atmospheric action is the most important factor providing variety of hydro physical fields (Kordzadze et al., 2008; Demetrashvili et al., 2008, Demetrashvili and Kvaratskhelia, 2012), which, in turn is reflected on the mixed layer structures.

Temperature and salinity fields are characterized by insignificant variability during mentioned time. They are presented at the time moment: 22:00h, 15^{st} of February and 10:00h, 17^{st} of February (see Fig. 2). It is clearly observed, sea water temperature at any horizons of 2–26 m is less, than at the depths 36–56m, especially, in the open part of sea basin (Fig. 2a). Unlike them, in east part of the Black sea, especially Georgian waters sea temperature decreases on the depth. It should be noted that the warm current within upper layer of the sea and heat flux directed from the sea to the atmosphere, near the Caucasian coast(in Sochi), in winter season are identified with high accuracy by Ratner and Korotaev (2017). The salinity fields in any cases are characterized by relatively high salinity waters in the cyclone

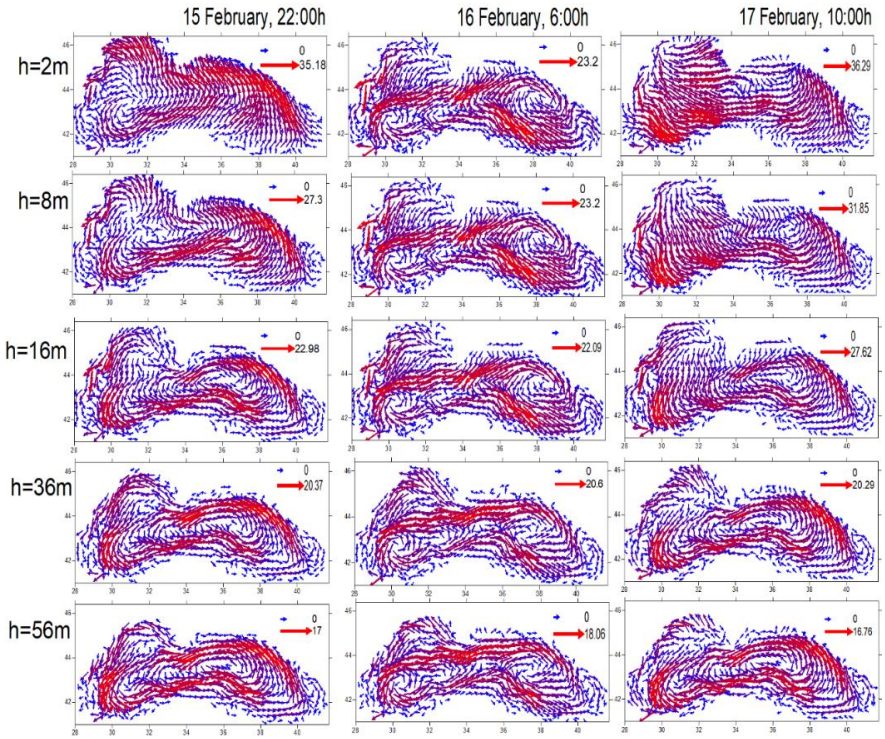

Figure 1. Simulated fields of Black Sea current(sm/s) on depth $h = 2, 8, 16, 36, 56$m, at the time moments: 15^{st} of February, 22:00 h; 16^{st} of February, 6:00h and 17^{st} of February, 10:00h.

centers, than at the periphery (see Fig. 2b), which in turn are related to the sea circulation structures on the vertical.

These simulated fields of the temperature and salinity in turn allow us to specify MLD using criterion of temperature ($0.2°C$) and salinity (0.15 psu). MLD variability accordance to the both criterions is illustrated on the Figures 3a and 3b respectively. As Figure 3a displays the strong mixing is progressed in the temperature fields from sea surface till 36–56m, in the open water part below of 44°N till the south coastal line, especially in the east part of the sea basin.

It is noticeable that the water area, in which MLD is 56m becomes wider in the east areas of sea for 10:00h, 17 February (see Fig. 3a). It coincides with the southeastern branch of Rim current (Fig. 1). This branch is distinguished by intensive flow near 40°E, right of which the anticyclonic vortex is observed in the same depth. Unlike it, MLD does not exceed 16 meter, above of 44°N. As mentioned, this numerical study is based on several climatic data corresponding to different time periods, which in turn reduce the ability to calibrate the model result by satellite images. Despite this, MLD in the temperature fields with coordinates: $30°8' - 31°9'$E, $42°27' - 43°03'$N is close to the results of the winter season obtained on the basis of experimental and model studies by Korotaev et al., (2011).

On the same Figure 3, MLD changeability is illustrated in the salinity fields, whose homogeneity is specified in the frame of 0.0–0.15 psu. Mixed layer maximal depth in mid-February using this criterion is approximately 30m (see Fig. 3b). Here, a relatively strong mixing is developed mainly in the north areas of the Black Sea basin above of 44°N, at the time moments: 22:00h, 15^{st} February and

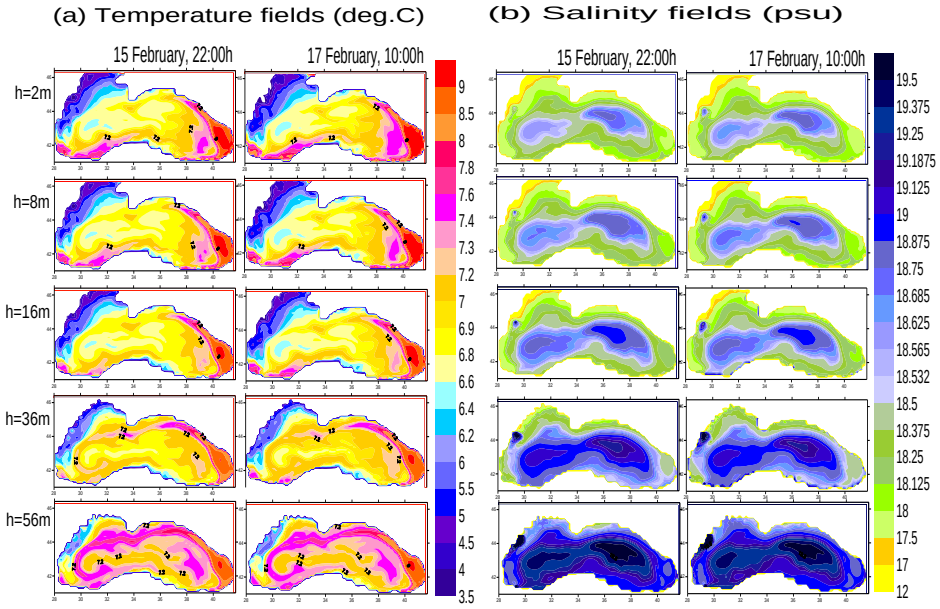

Figure 2. Simulated fields of temperature °C-(a) and salinity (psu)-(b) on depth $h = 2, 8, 16, 36, 56$m, at the time moments: 15^{st} of February, 22:00h and 17^{st} of February, 10:00h.

6:00h, 16^{st} February. This area on the basis our study, dos not stand out by intense anticyclones, but it is characterized with the buoyancy flux positive role in the mixed layer forming (evaporation exceeds precipitation). It should be noted that the active mixing areas of North-western and Crimean sea waters (see Fig. 3b) are identified as the best result of strong mixing in February using density criterion (0.07 kg/m^3) (Kubryakov et al., 2019). Besides, a relatively strong mixing from Sevastopol water area spreads till the western central part within the depth of 0–26m on 10.00h, 17^{st} of February (Fig. 3b). In the same vertical column, the cyclonic circulation is in process forming (Fig. 1) and the strong vertical gradient of the sea velocity caused by the intense wind-driven turbulence, in turn, intensifies mixed layer forming. Unlike it, in the areas of east central gyre, at the moment 10.00h, 17^{st} of February, mixed layer depth is relatively small. In our opinion, reduction mixed layer is caused by upraise of the pycnocline in relation to the sea circulation (Fig. 1). Besides, in the central part of the sea basin with coordinates: $34°5' - 36°5'$E; $43° - 44°$N, during the calm condition, at the time moment 6:00h, 16^{st} of February, mixed layer depth is a relatively small, than in the other open part of sea basin (see Fig. 3b). The same central part is characterized by minimal depth of the mixed layer using criteria sigma-t(density) (Kubryakov et al., 2018). In addition, this numerical result in the interior basin is a relatively good approaches to experimental date (Oguz, 2009), in which, the upper 50–60m homogeneity is estimated by 0.3 psu.

Here, on the Figures 4 and 5, the differences in the temperature and salinity fields ($\triangle T$ and $\triangle S$), between depths $z = 2, 8, 12, 16, 26, 36, 56$m and the sea surface (z=0 m), more clearly reflect the physical processes, which are developed in the mixed layer. It is obvious that at the time moment: 22:00h, 15 February and 6:00h, 16 February, in the case of relatively strong and calm winds respectively, the mixed layer is characterized by cooling process using the criterion of temperature (0.2°C),

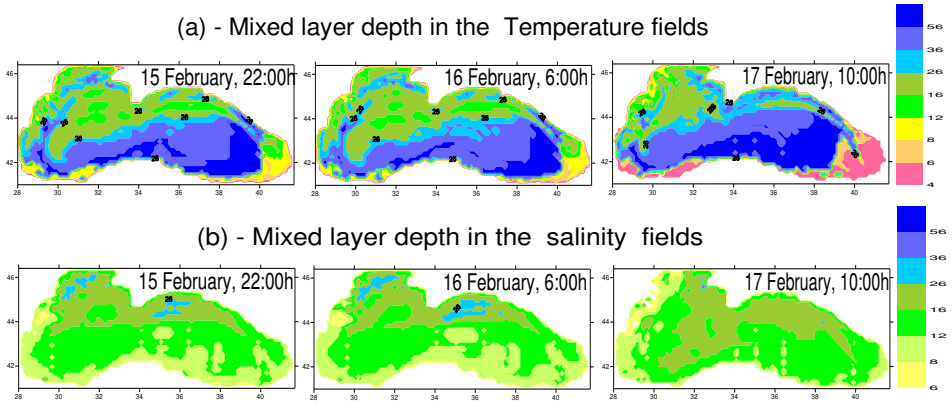

Figure 3. Simulated depth of mixed layer using criteria Temperature (0.2°C)-(a) and 0.15 psu for Salinity-(b) at the time moments: 15^{st} of February, 22:00h; 16^{st} of February, 6:00h and 17^{st} of February, 10:00h

which covers 0–2 meter and it spreads till 16m, in the north, north-western and its surrounding open water part of the sea (see Fig. 4). Moreover, within depth 16–56m, the cooling process is spreading till the south coastal line, especially in the central segments of the Turkish sea waters. It should be noted that in the north, north-western and the surrounding waters in the western central part, below of 16m, the differences of temperature on vertical exceeds 0.2°C. These areas are distinguished by strong cooling $0.2°C < \triangle T < 0.5$°C, which not fixed on the Figure 3a. In the same period of time between Bulgarian and Georgian coastal sea waters, sea temperature decreases on depth 2–56m. This process is more clearly observed within a depth 8–36m, but at same time, below of 16m, in sea waters near the Istanbul strait and in south-east coastal line as well as in the Georgian segment, the differences of temperature with relation to the sea surface exceeds 0.2°C. It should be noted in Figure 3a, in the same areas MLD does not exceed $16m$ using the criterion of the temperature 0.2°C. The areas of the warm pool, in which sea temperature decreases on the vertical are simulated with minimal heat fluxes and a lower speed of wind's in the Black Sea basin.

As it is observed, mixing process features are not changed in the case of the calm conditions at 6:00h, 16^{st} of February (see Fig. 4). In our opinion, it is related to the morning hours (6:00h), when sea water has almost the same temperature, which was accumulated in previous day evening hours (22:00h). Besides, this result demonstrates that: after strong wind, when weak wind is operated, sea circulation near the sea surface is transformed as cyclonic current system, which in short time has not ability to changes mixed layer features (Kvaratskhelia et al., 2018). In contrast, at 10:00h on 17 February in the morning hours, the solar radiation flux is reflected on the mixed-layered structures and the temperature on the sea surface is higher than at a depth of 2–8m (Fig. 4). Here, below 8 meters, the mixed layer at first glance has practically the same structure as in the previous time moments, but the areas in which the sea temperature is higher than at the sea surface within the framework of the criterion used (0.2°C) becomes relatively large below of 16 meters, especially in the eastern part of the sea, corresponding to the southeastern branch of Rim current, in which the maximum depth of the mixed layer is about 56m (see Fig. 3a).

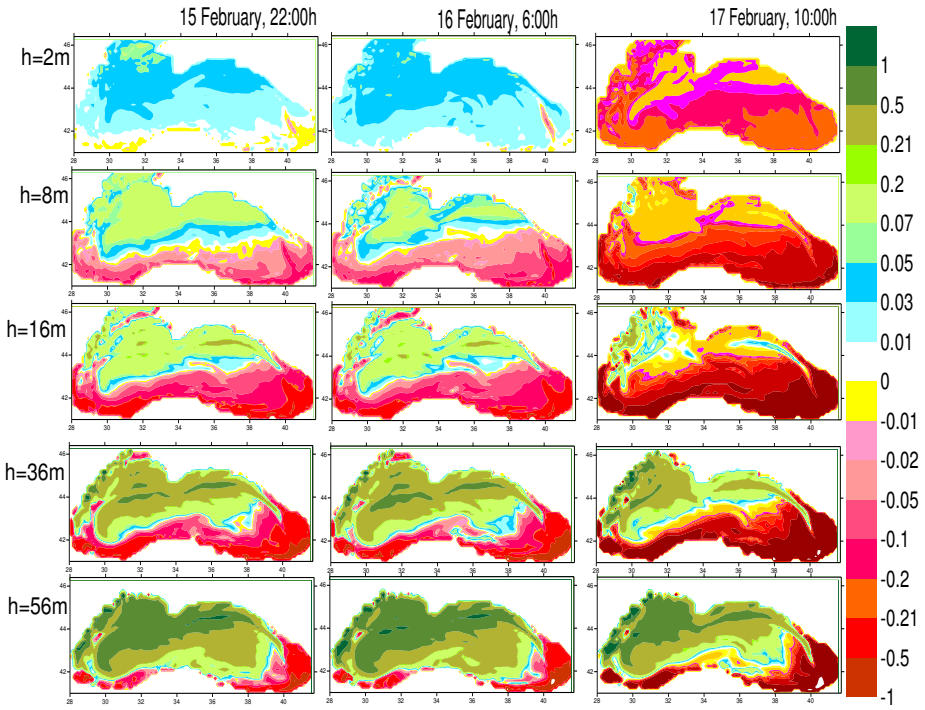

Figure 4. Differences in the temperature fields (°C), between depths $z = 2, 4, 6, 8, 16, 36, 56$m and the sea surface (z=0 m), at the time moments: 15^{st} of February, 22:00h; 16^{st} of February, 6:00h and 17^{st} of February, 10:00h.

At the same time, mixed layer in the salinity fields, within 0–2 meter, in which non-stratified structures are dominated basically (see Fig. 5), in turn, is agreed with the atmospheric and sea circulation processes (Fig. 1). Below 2 meters, sea salinity grows on the depth. Mixed layer was transformed as slightly stratified structures ($0.001\,\text{psu} \leq \triangle S \leq 0.15\,\text{psu}$) and its area decreased also, especially, from the depth 12m (see Fig. 5). Here, in the same Figure 5, mixed layer with the slightly stratified structures is observed in the north-wester and Crimea waters approximately till 30m, in the time interval: 15^{st} of February, 22:00 h–16^{st} of February, 6:00h. Besides, mixing process spreads in the open western part of sea for time moment 10:00h, 17^{st} of February (see Fig. 5). It is a good result of united action of both the strong wind and buoyancy flux.

As mentioned, mixed layer flexibility with regard to both values of Richardson Numbers: Ri_t and Ri_S are at the center of our attention. It is well known, these values in turn reflect the ratio between the stabilizing buoyancy forces (the Brunt-Vaisala frequency squares) and de-stabilizing shear forces. Here, in Figures 6 and 7, both values of Richardson Numbers: Ri_t and Ri_S are presented on the same above mentioned depths: $2, 8, 12, 16, 26, 36, 56$m. They are simulated in relation to the sea surface.

It is clear, near the sea surface, within 0–2 meters, the Richardson Number values Ri_t and the differences in the temperature fields ($\triangle T$) are well coordinated with each other (see Figures 6 and 4, respectively). Below 2 meters till 16 meters, in the same north, north-wester and they surrounding open central part, in which cooling processes are observed in frame of 0.2°C (see Fig. 4), the gradient of Richardson

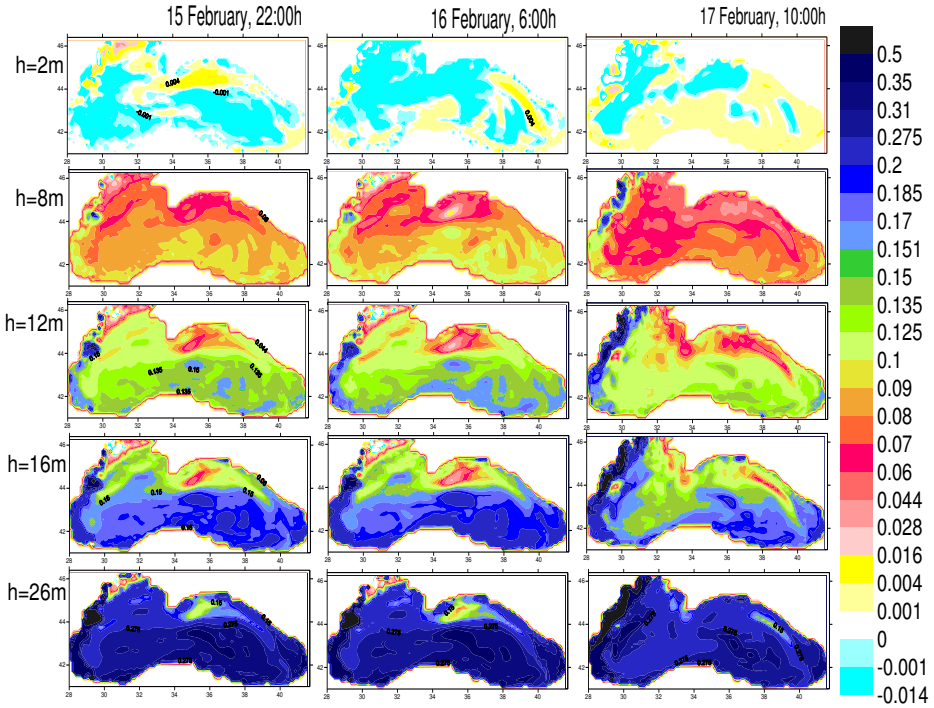

Figure 5. Differences in the salinity fields (psu), between depths $z = 2, 4, 6, 8, 12, 26$m and the sea surface (z=0 m), at the time moments: 15^{st} of February, 22:00 h; 16^{st} of February, 6:00h, and 17^{st} of February, 10:00h.

number basically is variable in range of $0.00002 \leq Ri_t \leq 1$ at the time moment 22:00h, 15^{st} of February (see Fig. 6).

It is easy to note that, within depth of 16–56 meters, in the same areas, in which as mentioned, the differences of temperature changed in range of $0.2°C < \triangle T \leq 0.5°C$ (see Fig. 4), Richardson number values is variable in frame of $1 < Ri_t \leq 10$ (see Fig. 6). Besides, within depth 8–36m, between Bulgarian and Georgian coastal sea waters and its surrounding open water part, in which sea temperature decreased in frame of $-0.01°C < \triangle T \leq -0.2°C$, when the depth increased, Ri_t is variable in frame of $-0.0001° < Ri_t \leq -1$. At the same time, at depths 36 and 56 meter, Ri_t values are changed in frame of $-10 \leq Ri_t < -100$, especially in the south-west (near of Istanbul strait) and in south-east coastal line, as well as in the Georgian sea waters, in which the differences of temperature changed in diapason $-0.2° < \triangle T < -0.5°C$. It should be noted, in the same context, that a better coherence between mixed layer structures and Richardson number values is observed at 10:00h, 17 February (see Fig. 4 and Fig. 6). Unlike them, in case of the weak wind action, on 6:00h, 16 February, below of 2m, in the same-North, North-western and they surrounding open central part, in which differences of temperature did not exceed 0.2°C, the gradient of Richardson number's is variable in in the following diapason $1 < Ri_t \leq 10$.

It is well known that the Richardson Number varying within $-1 < Ri_\rho < 0$, corresponds to the statistically unstable configuration (Bennis et al., 2008, 2010; Rubino, 2014). In our cases, non-stratified structures, in which $\triangle S$ varied in the range $-0.001\,\text{psu} \leq \triangle S \leq -0.014$ psu near the sea surface, within 0–2m (see

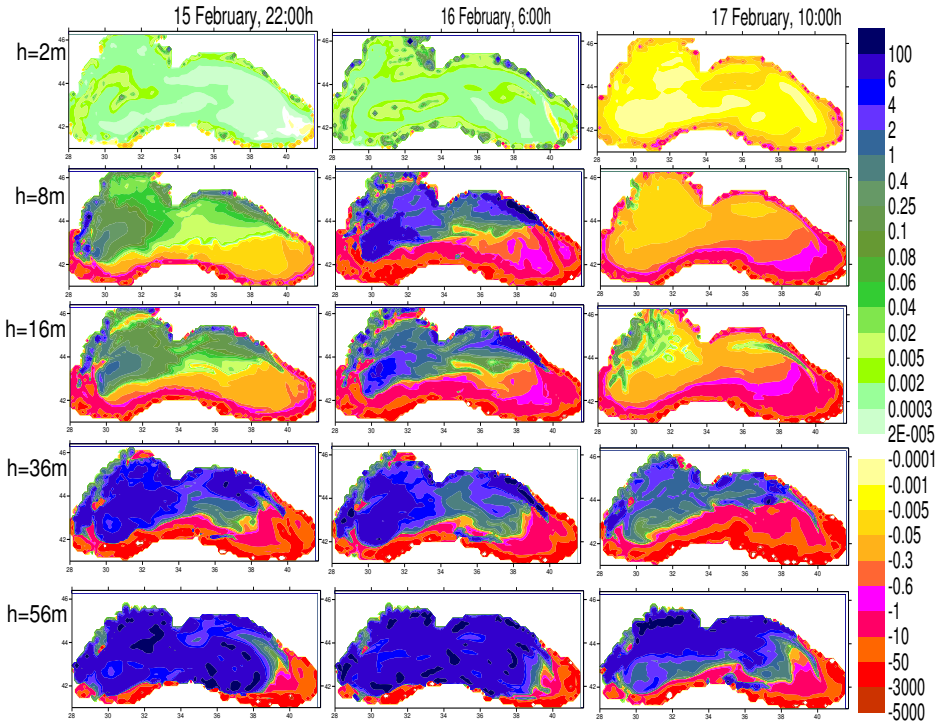

Figure 6. The Richardson number vertical distribution accordance to temperature fields-Ri_t, on the depth 2, 8, 16, 36, 56 meter in relation to sea surface, at 15^{st} of February, 22:00h; 16^{st} of February, 6:00h and 17^{st} of February, 10:00h.

Fig. 5), are in good correlation with the Richardson number, which changed in the range of $-0.00002 < Ri_s \leq -1$, during the above mentioned time period (22:00h, 15 February –10:00h, 17 February). In the same depth, the areas in which $\triangle S$ varied in range of $0.001\,\text{psu} \leq \triangle S \leq 0.004$ psu is an excellent result a slightly stable configuration's $0.000002 < Ri_S \leq 0.00007$. Below 2 m till 26 m, mixed layer with slightly stratified structures ($0.001\,\text{psu} \leq \triangle S \leq 0.15\,\text{psu}$) is in good agreement with the Richardson number, which changes in the diapason $0.000002 < Ri_S \leq 0,8$, on 22:00h, 15 February and at 10:00h, 17 February (see Fig. 5 and Fig. 7, respectively). As mentioned, within depth 12-26 m mixed layer area reduced, despite this, it is spreading from the north (Sevastopol and Crimean waters) till the western central part for the time moment 10:00h, 17 February (see Fig. 5). It is noticeably, here in the same depth, in the eastern open central part, in which the differences in the salinity exceed 0.15 psu, sea water is close to slightly stable configuration ($0.07 < Ri_S \leq 1$) (see Fig. 7). This result allows us to note: in case of the relatively strong wind action, mixed layer in the salinity fields, its homogeneity, especially in deep waters of the sea basin is more even sensitive to the Richardson numbers, than in the temperature fields.

Besides, as it is seen, in the case of the weak wind action, for the time moment: 6:00h, 16 February, mixed layer has almost same structures, which is fixed at 22:00h, 15 February. It is easy to notice that, at the same time, in the upper layer of the sea within depth 2–12m, in the south-western as well as in the south-east segments of the sea basin, in which differences in the salinity fields do not exceed

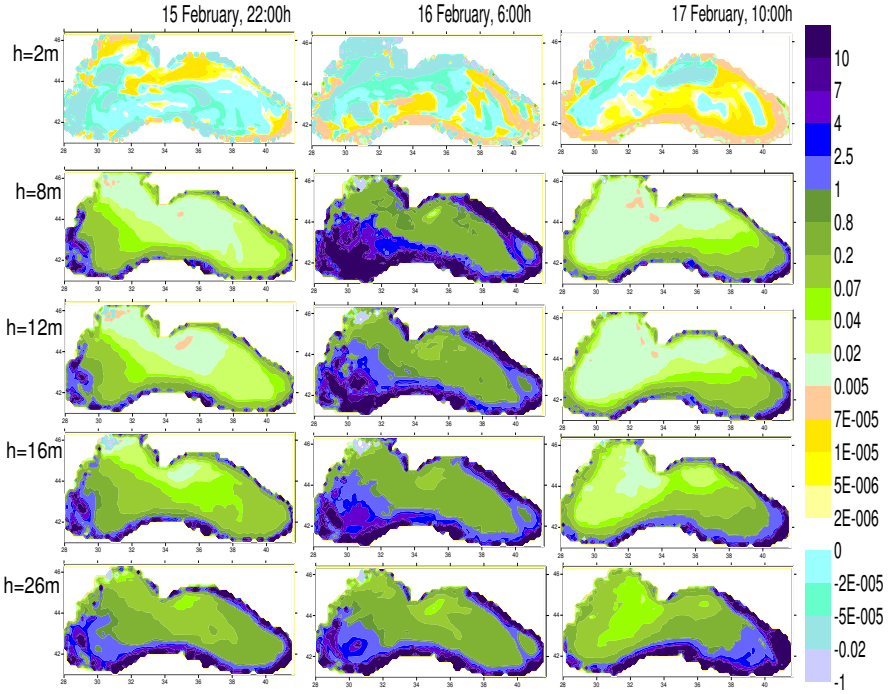

Figure 7. The Richardson Number vertical distribution accordance to the salinity fields-Ri_S, on the depth $2, 8, 12, 16, 26$m in relation to sea surface, at the time moments: 15^{st} of February, 22:00h; 16^{st} of February, 6:00h and 17^{st} of February, 10:00h.

0.15 psu (see Fig. 5), Richardson number is changed in the following diapason $1 < Ri_S \leq 10$ (see Fig. 7). As above mentioned, in calm condition, in North, North-west and western central part of sea basin the same tendency is observed: Richardson number changes within $1 < Ri_t \leq 10$, when differences of the temperature do not exceed 0.2°C (see Fig. 4 and Fig. 6, respectively). This is a clear example of Richardson number sensitivities to both strong and weak winds actions, which, in turn demonstrates that, in the case of strong winds, mixed layer structures (in winter season) are in good coherence with the values of the Richardson number.

7. Conclusion

Mixed layer investigation in the Black Sea basin were carried out on the basis BSM-IG, improved using new model of the PP parameterization formulated by Bennis et al.(2010) for VTV and VTD coefficients.

Here, mixed layer main elements are presented on the example of mid-February (winter season). As the analysis of numerical experiments show: MLD in the temperature fields, according to the temperature criterion (0.2°C), from sea surface reaches 36–56m, in the open waters below of 44°N till the south coastal line. Its maximal depth 56m coincides with the south-eastern branch of Rim current's for 10:00h, 17 February (Fig. 3a). This branch close to 40°E distinguished with the intensive flow, right of which in the same depth the anti-cyclonic vortex is observed (Fig. 1). Mixed layer homogeneity in the salinity fields is specified in frame of 0.0–0.15 psu. MLD in the mid-February using this criterion does not exceed 30m (Fig. 3b). Here, a relatively strong mixing develops in north area of the Black Sea

basin, which is spreading from the Sevastopol water areas till the central part of the west, in a mentioned time: 22:00h, 15^{st} of February –10:00h, 17^{st} of February. It should be noted, that this area is characterized by the buoyancy flux positive role (evaporation exceeds precipitation) and winds intensity.

In additionally, the differences in the temperature and salinity fields on the several depth in relation to the sea surface more clearly illustrate some aspect of the mixed layer. Among them, the strong mixing-cooling process covers all the most north, north-western and its surrounding western central areas in frame of 0.2–0.5°C, within range of the depth 16–56m (Fig. 4). The mentioned areas of the sea basin are characterized by both maximal heat flux and winds intensity. Besides, at morning 10:00h, 17^{st} of February, solar radiation flux is reflected on the mixed layer structures and sea temperature decreases in frame of 0–0.2°C on the depth 0–8m. At the same times of February, non-stratified structures mainly dominate within 0–2 meters in salinity fields. Below 2 meters, mixed layer is transformed as a slightly stratified structures, which is identified in the frame of $0.01\,\text{psu} \leq \triangle S \leq 0.15\,\text{psu}$ (Fig. 5).

This study is a clear example of Richardson number's sensitivity to both strong and weak wind actions, which, in turn, demonstrates that, in the case of strong winds, mixed layer structures in good coherences with the specificity of Richardson number are generated (see Fig. 4, 5 and Fig. 6, 7, respectively).

Besides, this numerical experiment allow us to note, that, in the case of the relatively strong wind action, mixed layer in the salinity fields, its homogeneity is even more sensitive to the Richardson number's, than in the temperature fields. As far as, below 12m, mixed layer area in the salinity fields is reduced in the Black Sea basin, when Richardson number is changed in the following range $0.07 < Ri_S \leq 1$.

Acknowledgements.

This work has been supported by the Shota Rustaveli National Science Foundation Grant FR17_279.

References

[1] *Atlas of Excitement and a Wind of the Black Sea* (Russian), Gidrometeoizdat, Leningrad, (1969), 112 pp.

[2] M.I. Budyko, *Heat Balance of Earths Surface* (Russian), Gidrometeoizdat, Leningrad (1956), 254 pp.

[3] A.C. Bennis, T. Chacón-Rebollo, M. Gómez-Mármol and R. Lewandowski, *Stability of some turbulent vertical models for the ocean mixing boundary layer*, Appl. Math. Lett., **21** (2008), 128-133. https://doi.org/10.1016/j.aml.2007.02.016

[4] A.C. Bennis, T. Chacón-Rebollo, M. Gómez-Mármol and R. Lewandowski, *Numerical modelling of algebraic closure models of oceanic turbulent mixing layers*, ESAIM-Math. Model., **44** (2010), 1255-1277. https://doi.org/10.1051/m2an/2010025

[5] A. Capet, C. Troupin, J. Carstensen, M. Grégoire & J-M. Beckers, *Untangling spatial and temporal trends in the variability of the Black Sea Cold Intermediate Layer and mixed Layer Depth using the DIVA detrending procedure*, Ocean Dynamics, **64**, 3 (2014), 315-324. https://link.springer.com/article/10.1007/s10236-013-0683-4

[6] T. Chacón-Rebollo, M. Gómez-Mármol and S. Rubino, *Numerical investigation of algebraic oceanic turbulent mixing-layer models*, Nonlin. Processes Geophy., **20** (2013), 945-954. https://doi.org/10.5194/npg-20-945-2013

[7] T. Chacón-Rebollo, M. Gómez-Mármol and S. Rubino, *Analysis of numerical stability of algebraic oceanic turbulent mixing layer models*, Applied Mathematical Modelling, **38**, 24 (2014), 5836-5857. https://doi.org/10.1016/j.apm.2014.04.050

[8] D.I. Demetrashvili, D.U. Kvaratskhelia and A.I. Gvelesiani, *On the vortical motions in the Black Sea obtained by the 3-D hydrothermodynamical numerical model*, Adv. Geosci., **14** (2008), 295-299. https://doi.org/10.5194/adgeo-14-295-2008

[9] D.I. Demetrashvili, D.U. Kvaratskhelia, *Numerical study of the vertical hydrological structure of the Black Sea under transitive climatic forcing conditions*, Bulletin of the Georgian National Academy of Sciences, Geophysics, **6**, 2 (2012), 83-88. http://science.org.ge/old/moambe/6-2/83-88%20Demetrashvili.pdf

[10] D. Demetrashvili, V. Kukhalashvili, A. Surmava, D. Kvaratskhelia, *Modeling of Variability of the Regional Dynamic Processes Developed During 2017-2019 in the Easternmost Part of the Black Sea*, GEOLINKS Conference, (2020)

[11] H.J. Friedrich and E.V. Stanev, *Parameterization of vertical diffusion in numerical model of the Black Sea, Small sea turbulence and mixing in the ocean*, Elsevier Oceanography Series, **46** (1988), 151-167

[12] R.W. Helber, A.B. Kara, C.N Barrona. T.P. Boyer, *Mixed layer depth in the Aegean, Marmara, Black and Azov Sea, Part II: Relation to the sonic layer depth*, Journal of Marine Systems, **78** (2009), S181-S190

[13] A.B. Kara, A.J. Wallcraft and H.E. Hurlburt, *A new solar radiation penetration scheme for use in ocean mixed layer studies: an appilication to the Black Sea using a fine-resolution hybrid coordinate ocean model (HYCOM)*, J. Phys. Oceanog., **35** (2005a), 13-32

[14] A.B. Kara, H.E. Hurlburt, A.J. Wallcraft and M.A Bourassa, *Black Sea mixed layer sensitivity to various wind and thermal forcing products on climatological time scales*, J. Climate, **18** (2005c), 5266-5293

[15] A. Kordzadze, K. Tavartkiladze and D. Kvaratskhelia, *A structure of the wind continuous field on the Black Sea surface*, J. Georgian Geophys. Soc., **5b** (2000), 28-37.

[16] A.A. Kordzadze, D.I. Demetrashvili and A.A. Surmava, *Numerical Modeling of Geophysical Fields of the Black Sea under the Conditions of Alternation of Atmospheric Circulation Processes*, Izvestiya, Atmospheric and Oceanic Physics, **44**, 2 (2008/1), 213-224

[17] A.A. Kordzadze, D.I. Demetrashvili, A.I. Gvelesiani and D.U. Kvaratskhelia, *On the vortical motions in different turbulent layers of the Black Sea*, J. Georgian Geophys. Soc., **5b**, 12 (2008/2), 17-35

[18] A.A. Kordzadze and D.I. Demetrashvili, *Operative forecast of hydrophysical fields in the Georgian Black Sea coastal zone within the ECOOP*, Ocean Sci., **7** (2011), 793-803. https://doi.org/10.5194/os-7-793-2011

[19] G. Korotaev, T. Oguz, A. Nikiforov and C. Koblinsky, *Seasonal, interannual, and mesoscale variability of the Black Sea upper layer circulation derived from altimeter data*, J. Geophys. Res., **108**, 4, 3122 (2003), 16pp. https://doi.org/10.1029/2002JC001508

[20] G.K Korotaev, T. Oguz, V.L. Dorofeyev, S.G. Demyshev, A.I. Kubryakov and Yu.B. Ratner, *Development of Black Sea nowcasting and forecasting system*, Ocean Sci., **7** (2011), 629-649. https://doi.org/10.5194/os-7-629-2011

[21] G.K. Korotaev, V. Knysh, P. Lishaev, S.G. Demyshev, *Application of the Adaptive Statistics Method for Reanalysis of the Black Sea Fields Including Assimilation of the Temperature and Salinity Pseudo-Measurements in the Model*, Physical Oceanography, **1**, 25 (2018), 36-51 DOI: 10.22449/1573-160X-2018-1-36-51

[22] A.I. Kubryakov, G.K. Korotaev, V.L. Dorofeev, Y.B. Ratner, A. Palazov, N. Valchev, V. Malciu, R. Mateescu and T. Oguz, *Black Sea coastal forecasting system*, Ocean Sci., **8** (2012), 183- 196. https://doi.org/10.5194/os-8-183-2012

[23] A.A. Kubryakov, V.N. Belokopytov, A.G. Zatsepin, S.V. Stanichny, V.B. Piotukh, *The Black Sea Mixed Layer Depth Variability and Its Relation to the Basin Dynamics and Atmospheric Forcing*, Physical Oceanography, **26** (2019), 397-413. DOI: 10.22449/1573-160X-2019-5-397- 413

[24] D.U. Kvaratskhelia, K.Z. Chargazia and D.I. Demetrashvili, *Numerical investigation of the upper biologically acting turbulent layer of the Black Sea*, International Scientific Conference, Modern Problems of Ecology, Proceedings, **6** (2018), 51-54. http://dspace.gela.org.ge/handle/123456789/7284

[25] O.I. Mamaev, Simplified relationship between the density, *Temperature, and Salinity of Seawater*, Izv. Akad. Nauk SSSR, Ser. Geofiz., **2** (1964), 309-311.

[26] G.I. Marchuk, *Numerical Solution of the Problems of the Atmosphere and the Ocean Dynamics*, Gidrometeoizdat, (1974), 303 pp.

[27] G.I. Marchuk, *Methods of Numerical Mathematics*, 2nd ed., Nauka, Moscow, (1980); Springer, New York, (1982), 524 pp.

[28] G. Monterey and S. Levitus, *Seasonal variability of mixed layer depth for the world ocean*, NOAA Atlas NESDIS, Natl. Oceanic and Atmos. Admin., Silver Spring, Md., **14** (1997), 100 pp.

[29] M.E. Mihailov, S. Stefan, V. Diaconu, L. Lazar, *Longterm variability of the water mass structure on the romanian black Sea shelf*, Romanian Reports in Physics, **68**, 1 (2016), 377-392. http://www.rrp.infim.ro/2016_68_1/A32.pdf

[30] T. Oguz, H. Ducklow, P. Malanotte-Rizzoli, J.W. Murray, V.I. Vedernikov, U.A. Unluata, *Physical-biochemical model of plankton productivity and nitrogen cycling in the Black Sea*, Deep Sea Research, **46** (1999a), 597-636.

[31] T. Oguz, J. W. Murray and A. Callahan, *Simulation of Suboxic-Anoxic interface zone structure in the Black Sea*, Deep Sea Research, **48** (2001a), 761-787.

[32] T. Oguz, *State of the Environment of the Black Sea (2001-2006/7)*, Publications of the Commission on the Protection of the Black Sea Against Pollution (BSC) 2008-3, (2008), 421 pp. https://www.cbd.int/doc/meetings/mar/ebsaws-2017-01/other/ebsaws-2017-01-bsc-submission-05-en.pdf

[33] R.C. Pacanowski and S.G.H. Philander, *Parameterization of vertical mixing in numerical models of tropical oceans*, J. Phys. Oceanogr., **11** (1981), 1443-1451. https://doi.org/10.1175/1520-0485(1981)011¡1443:POVMIN¿2.0.CO;2

[34] A.E. Pogrebnoi, A.S. Samodurov, *Evolution of mixed layers in a stratified region of the Black Sea anticyclonic eddy*, Izvestiya Atmospheric and Oceanic Physics, **50**, 6 (2014), 621-629. doi.org /10.1134/S0001433814060127

[35] Yu.B. Ratner, G.K. Korotaev, *Specific features of heat exchange between the Black Sea and the atmosphere in winter in 1971-1991*, Russian Meteorology and Hydrology, **42** (2017), 503-509. DOI: 10.3103/S1068373917080039

[36] S. Rubino, *Numerical modeling of turbulence by Richardson-number based and VMS models* (2014), 194.
https://pdfs.semanticscholar.org/c6de/d70246ee260592a5360c60fa705cfacf9a3e.pdf

[37] E. Rusu, *Strategies in using numerical wave models in ocean/coastal applications*, Journal of Marine Science and Technology, **19**, 1 (2011), 58-75.

[38] E. Rusu, *Study of the wave energy propagation patterns in the western Black Sea*, Applied Sciences, **8**, 6, 993 (2018), 17 pp. https://doi.org/10.3390/app8060993

[39] L. Rusu, *The wave and wind power potential in the western Black Sea*, Renewable Energy, **139** (2019/1), 1146-1158

[40] L. Rusu, *Evaluation of the ear future wave energy resources in the Black Sea under two climate scenarios*, Renewable Energy, **142** (2019/2), 137-146

[41] J.V. Staneva and E.V. Stanev, *Oceanic response to atmospheric forcing derived from different climatic data sets, inter-comparison study for the Black Sea*, Oceanologia Acta, **21** (1998), 383-417

[42] E.V. Stanev, *Understanding Black Sea dynamics, an overview of recent numerical modeling*, Oceanography, **18**, 2 (2005), 56-75

[43] E.V. Stanev, Y. He, J. Staneva and E. Yakushev, *Mixing in the Black Sea detected from the temporal and spatial variability of oxygen and sulfide - Argo float observations and numerical modelling*, Biogeosciences, **11** (2014), 5707-5732 doi:10.5194/bg-11-5707-2014

[44] R.O.R. Thompson, *Climatological models of the surface mixed layer of the ocean*, J. Phys. Oceanogr., **6** (1976), 496-503

[45] L.I. Sukhikh, V.L. Dorofeyev, *Influence of the vertical turbulent exchange prameterization on the results of reanalysis of the Black Sea hydrophysical fields*, Physical Oceanography, **25**, 4 (2018), 262-269. DOI: 10.22449/1573-160X-2018-4-262-279